

Measuring microscopic viscosity with optical tweezers as a confocal probe

Boaz A. Nemet and Mark Cronin-Golomb

We demonstrate, what is to the best of our knowledge, a new method for studying the motion of a particle trapped by optical tweezers; in this method the trapping beam itself is used as a confocal probe. By studying the response of the particle to periodic motion of the tweezers, we obtain information about the medium viscosity, particle properties, and trap stiffness. We develop the mathematical model, demonstrate experimentally its validity for our system, and discuss advantages of using this method as a new form of scanning photonic force microscopy for applications in which a high spatial and temporal resolution of the medium viscosity is desired. © 2003 Optical Society of America

OCIS codes: 180.5810, 180.1790, 170.3880, 140.7010.

1. Introduction

In the study of colloidal suspensions and polymer physics and in molecular and cell biology it is often desirable to have a direct observation in real time of the changes in the local viscosity that affect the dynamics of such objects as colloidal particles, cellular organelles, and macromolecules. For example, in cell biology the study of intercellular signaling is advancing rapidly.¹ Tissue function heavily depends on the ability of neighboring cells to communicate. Cells communicate primarily by secreting cytokines, which are soluble proteins that diffuse through the surrounding medium and ultimately bind to receptors where the signal is received.² These signals modulate the functional activities of individual cells and tissue. The diffusion of the signaling molecules is governed by the gradients in concentration and viscosity in the intercellular medium. Mapping the viscosity in such a medium is therefore important for understanding the processes involved in intercellular signaling that could have considerable implications for the interpretation of organ physiology and for tissue engineering.

When this research was performed the authors were with the Department of Biomedical Engineering, Tufts University, 4 Colby Street, Medford, Massachusetts 02155. M. Cronin-Golomb (Mark.Cronin-Golomb@tufts.edu) is currently with Biological Sciences, Columbia University, 1002 Fairchild Center, MC 2435, New York, New York 10027.

Received 11 June 2002; revised manuscript received 2 December 2002.

0003-6935/03/101820-13\$15.00/0

© 2003 Optical Society of America

Recently we have demonstrated³ that quantitative mapping of viscosity distributions can be achieved with a high spatial and temporal resolution by using a method that probes such viscous environments by use of photonic force. In that previous research, we have obtained a detailed map (0.5- μm resolution) of the relative viscosity in the extracellular environment of a high-molecular-weight-biopolymer-producing cell of *Aureobasidium pullulans*. In this paper we expand on the experimental and theoretical basis of this method and discuss advantages, limitations, and extensions, such as dynamic light scattering and flow and force measurements.

Optical tweezers have proved a powerful tool in the investigation of biological systems, and many intriguing experiments have been performed on the physics of single molecules (for reviews see, for example, Ref. 4 and references therein). Optical tweezers allow noninvasive probing and manipulation of cellular environments. In our device, we use the trapped particle as the probe to measure the local viscosity. We approach the detection of that particle in what is to the best of our knowledge, a new way that employs confocal optics. The use of confocal geometry is a natural choice since the setup for optical tweezers is so similar to the setup for confocal microscopy. It results in sensitive detection and facilitates fast scanning and beam steering. In this design, the optical tweezers is also the probe beam of an inverted confocal microscope. The trapped object scatters light from the focal region and is confocally detected through a pinhole (or an optical fiber) placed in an image plane. To measure viscosity, we force the trapped particle periodically by moving the laser

tweezers back and forth across it at frequencies in the kilohertz range at small amplitudes (~ 100 nm). This forcing results in periodic motion of the particle with the same frequency as the driving frequency and a phase lag due to the drag. By measuring this phase lag, we can determine the characteristic time constant of the motion, which is proportional to the medium viscosity. If at the same time the particle is moved through the field of view, a spatial map of the viscosity is obtained. If this is repeated at different times and at different depths, we have a full three-dimensional (3-D) mapping of the viscosity distribution and evolution.

The outline of the paper is as follows. In Section 2 we describe the experimental procedure and the optical setup. In Section 3 we elaborate on some of the optical design considerations. In Section 4 we develop the physical model from first principles to the analytical solution, which is the main result and the basis of the measurement technique. The analytical solution is derived from a linearized equation under nonrestrictive simplifying assumptions. In Section 5 we show results from theoretical research on the signal-to-noise ratio (SNR) and its dependence on the various parameters, as well as a comparison with experimental SNR. In Section 6 we show the change in trap stiffness with depth within the specimen and give an interpretation of it in terms of optical aberrations. Section 7 is the discussion. In Subsection 7A we review some of the existing methods and show similarities to and differences from our own method, and in Subsection 7B we discuss extensions to the method, such as localized dynamic light-scattering microscopy and flow measurement. Finally, we conclude in Section 8 with a summary of the main results, followed by an appendix detailing the signal-to-noise calculations.

2. Experimental Setup and Procedure

Figure 1 shows a schematic diagram of the optical layout. Linearly polarized light from a continuous wave (cw) Ti-Sapphire laser (Spectra Physics 3900, Mountain View, California) is focused by an objective lens (Edmunds Micro Plan 100×1.25 NA, Edmund Industrial Optics, Barrington, New Jersey) to form the optical trap in the sample. An acousto-optic deflector (AOD) (Isomet 1205C-2, Isomet Corporation, Springfield, Virginia) sets the beam into periodic motion, causing a trapped probe bead to oscillate in the transverse direction (only the first-order diffracted beam is used, whereas the zero order is blocked). Backscattered light from the trapped particle is descanned by the AOD and is detected confocally by placement of a pinhole or single-mode fiber near an image plane in front of the photodetector.⁵ The trapped particle appears as an object in the focal point of the laser beam. As the particle moves about in the trap, the confocal signal varies. For a well-aligned TEM₀₀ Gaussian beam the signal is maximum at the center and decreases as the particle moves away from the focal region. Because of the hydrodynamic drag, the particle lags behind the os-

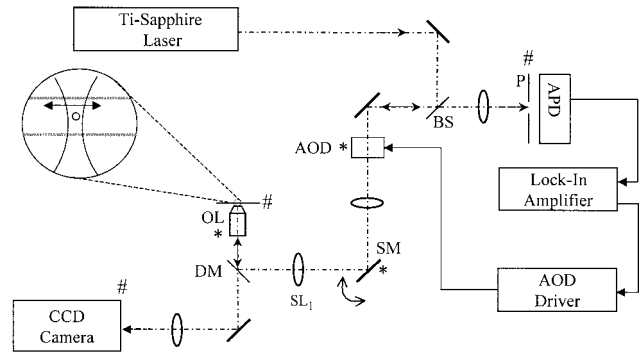


Fig. 1. Experimental layout. The pinhole (P) is placed in an image plane of the object, forming the confocal detection. These conjugate planes are marked with #. The AOD is placed at an optically conjugate plane of the back aperture of the objective lens (OL). The conjugate planes are marked with *. Two galvanometer SMs are placed in another such conjugate plane (*). The LIA drives the AOD with a sinusoidal waveform and measures the magnitude and phase of the APD signal at the second-harmonic frequency. The scene is viewed with a CCD camera in transmission through the dichroic mirror (DM) that has high reflectivity in the IR. SL_1 is the scan lens.

cillating beam. As a result, the beam traverses the particle twice in each cycle, and the confocal signal peaks twice per cycle, yielding a signal at the second harmonic.

A digital lock-in amplifier (LIA) measures the phase difference between the confocal signal and the second harmonic of the spatial oscillation frequency of the trap. The phase is then used to determine the local viscosity with the model in Section 4. The frequency and amplitude of the oscillations are set digitally by the LIA, which is used also as the function generator to supply the sinusoidal voltage to modulate the AOD carrier frequency.⁶

Two orthogonal scanning mirrors at location SM in Fig. 1 have four functions:

1. They can be used to form an image by x - y raster scan in the conventional use of the scanning confocal microscope.
2. They can be used to drag the particle in the sample, and with our measurement technique, to obtain an image of the viscosity.
3. They can be used to control and manipulate the laser trap's position. To accomplish this, we use our own computer software that integrates the CCD camera, the frame grabber, and the galvanometer drivers and allows us to take measurements of the viscosity at desired locations in the field of view. We use the computer mouse for the manipulation of the trap in real time by moving a cross hair on the computer screen. The mouse coordinates are translated into mirror coordinates by a linear transformation and sent through the serial port to the x - y galvanometer drivers.
4. They can be used to manipulate biological cells, possibly for sorting, in applications in which the viscosity measurement is used as an indicator of high-producing cells.

3. Optical Design

Optical tweezers and confocal geometry combine in a very natural and almost obvious way that is easy to implement. This arrangement is appealing for two main reasons: (i) for detection purposes in that the particle whose position we wish to detect is automatically aligned with the beam since we use the same laser beam for both detection and trapping and (ii) for steering capabilities in that the same optical design considerations that need to be addressed during construction of a steerable laser trap appear during construction of a confocal scanning laser microscope. The confocal design problem is how to move the beam at the sample plane without it walking off the back aperture of the objective lens, which would cause a reduction in light intensity and severe aberrations. By solving the confocal design problem, we also solve the problem for the steerable tweezers.

The standard solution in designing a confocal microscope is to place the scan mirror or any other steering device (e.g., AOD) at an optically conjugate plane to the back focal plane of the objective lens.^{7,8} In our case, a slight modification is to image the steering device onto the back aperture of the objective lens.⁹ This facilitates laser scanning with minimal loss of light and minimum aberrations since minimal lateral translation of the beam occurs at such a plane [marked with an asterisk (*) in Fig. 1]. In practice this is implemented with a scan lens (SL) that has three functions: (i) imaging the SM onto the objective lens back aperture; (ii) focusing the laser beam to a spot at a primary image plane, which is translated to a spot at the object plane by the objective lens (the optical trap); and (iii) overfilling the objective lens aperture by approximately 30% to ensure a diffraction-limited spot size,⁷ as required for a 3-D stable single-beam trap. Therefore, the focal length of the SL must satisfy the condition to yield the desired magnification for the beam width at the objective lens aperture.

The three conditions can be stated in mathematical form as a system of three simultaneous equations for the parameters f_1 , u_1 , and v_1 , which are respectively the SL focal length, the SM to SL₁ distance, and the SL to objective aperture distance.

- (i) $l/f_1 = l/u_1 + l/v_1$,
- (ii) $v_1 = 150 \text{ mm} + f_1$,
- (iii) $v_1/u_1 = M$,

where we used for (i) the image formation formula for a thin lens; for (ii), according to the DIN standard, the distance from the back aperture of the objective lens to the primary image plane is 150 mm, and we assumed that the beam is collimated before the SL; for (iii) the magnification M is known from the width of the beam before the lens and the size of the objective lens pupil. For example, with a 2-mm-diameter beam and 6-mm-diameter pupil, we get $M = 1.3 \times 6/2 = 3.9$.

Note that if the beam is not collimated before the SL then the calculation is a little more complicated, but we can still solve a system of simultaneous equations, taking into consideration the beam divergence, to obtain the information on the position of the SL and its focal length. Another consideration is the diameter of the SL. Since this lens also collects the backscattered light from the trapped object (or alternatively the fluorescence light), it should be as large as possible for high throughput to optimize the amplitude of the detected signal.

4. The Model

In confocal detection we receive a signal from the particle whenever it is in the focal region of the trapping beam. We therefore develop a mathematical model for $u = x - p$, where x is the transverse position of the particle and p is the trap position.¹⁰ We expect a peak in the signal whenever $u = 0$.

In the following, we describe the main features of our physical model that relate the measured phase and the microscopic viscosity. A particle trapped by the light force finds itself in, to a good approximation, a quadratic potential well (in the transverse direction). In this paper, we will consider the analysis of Newtonian fluids, noting that it is straightforward to make an extension to cases for which the Stokes–Einstein relation may be generalized to account for viscoelasticity.¹¹ In that case, the measured magnitude of the viscosity becomes frequency dependent. The generalized analysis is described elsewhere.

The one-dimensional (1-D) equation of motion of a particle in a viscous Newtonian fluid undergoing Brownian motion in an oscillating harmonic potential is

$$\gamma \frac{dx}{dt} + \kappa[x - p(t)] = L(t), \quad (1)$$

where x is the particle's position, $p(t)$ is the time-dependent position of the trap $p(t) = a \sin(\omega_0 t)$, and γ is the hydrodynamic drag coefficient. For a sphere far from any surface, γ is given by the Stokes formula $6\pi\eta r$, where r is the radius of the sphere and η is the dynamic viscosity.¹² $L(t)$ is the Langevin forcing function associated with Brownian motion, and κ is the tweezers spring constant. The inertial term (mass times acceleration) that would normally be included on the left-hand side of Eq. (1) can be neglected on the grounds that in common fluids the motion of micrometer-sized particles takes place at a small Reynolds number where viscous drag dominates inertial forces.¹² In terms of u , Eq. (1) becomes

$$\gamma \frac{du}{dt} + \kappa u = -\gamma a \omega_0 \cos \omega_0 t + L(t). \quad (2)$$

The assumption that the particle stays near the center of the trap also allows us to express the confocal signal as proportional to $1 - \alpha u^2$, where α is an expansion coefficient. In our measurement tech-

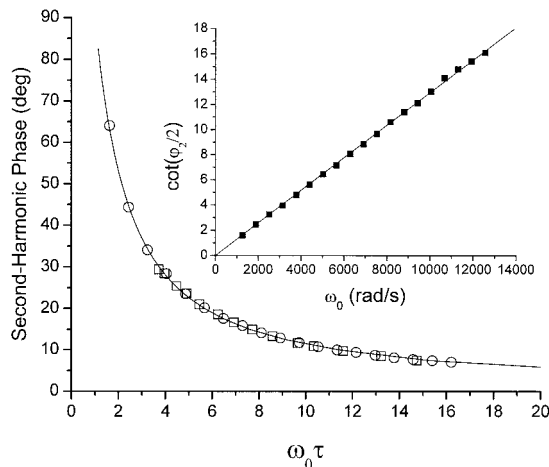


Fig. 2. Experimentally measured second-harmonic phase for 1.9- μm diameter silica microsphere in water, for varying laser power (15 to 60 mW at the sample) at a constant frequency of 600 Hz (\square) and for varying frequency (200 to 2000 Hz) at a constant power of 46 mW (\circ). Each measurement of ϕ_2 is the average of 512 samples from the LIA (sampled at 64 Hz). The LIA time constant was 100 ms, corresponding to NEBW of 0.78 Hz. The errors in ϕ_2 from the standard deviations are smaller or equal to the size of the symbols and are omitted for clarity. Both sets of measurements are plotted together after a linear regression fit was done on each set separately to obtain b . The abscissa parameter $\omega_0\tau$ is calculated from $\omega_0 b/P$. The solid curve shows the theoretical curve for which the x axis is $\cot(\phi_2/2)$. Inset: Linear regression fit to the frequency data, $\tau = 1.290 \pm 0.003$ ms with a correlation coefficient 0.99974. From a similar linear regression (not shown), we obtain for the power measurements $b = 59.48 \pm 0.27 \mu\text{J}$ with a correlation coefficient 0.999.

nique, the dominant forcing comes from the periodic motion of the tweezers, and we detect only the motion associated with this periodicity in a narrow band set by the time constant of the LIA. The contribution of the Brownian motion in such a narrow band of frequencies is small but is the main source of noise. Therefore we solve the equation without the Langevin term and consider it only later in the discussion of the SNR. The solution of Eq. (2) is

$$u(t) = -u_0 \sin(\omega_0 t + \phi_1), \quad (3)$$

where $\phi_1 = \cot^{-1} \omega_0\tau$ ($\tau = \gamma/\kappa$ is the relaxation time) and $u_0 = a\omega_0\tau/[1 + (\omega_0\tau)^2]^{1/2}$.

We find that the phase of the second harmonic appearing in u^2 is given by

$$\phi_2 = 2\phi_1 = 2 \cot^{-1} \omega_0\tau. \quad (4)$$

We verified the validity of our model by measuring the second-harmonic phase (ϕ_2) as a function of the laser power (P) and the trap oscillation frequency (ω_0). Figure 2 shows the results from two sets of measurements on a 1.9- μm -diameter silica microsphere in water. In one set of measurements, we keep the frequency of the oscillations constant (600 Hz) while varying the laser power between 15 and 60 mW. In the second set, the laser power is kept constant (46 mW at the sample) while the oscillation

frequency is varied between 200 and 2000 Hz. If the theory is correct and the trap spring constant is approximately proportional to power $\kappa = \kappa_0 P$, where P is the laser power, then decreasing the power is equivalent to increasing the oscillation frequency. We can therefore collapse the data on one graph and plot both sets as a function of the normalized time constant $\omega_0\tau$.

The parameter b , which is defined by $b = \tau P$, has units of energy and is a characteristic constant of the physical conditions of the experiment. It is independent of the frequency of the oscillations and the laser power (note that by definition τ is inversely proportional to κ , which by our assumption is proportional to P). This independence means that b remains constant for a given particle (size, shape, and refractive index), the fluid medium (viscosity and refractive index), and the optical microscope system being used (objective lens, laser mode, wavelength, etc.). We interpret it as the amount of electromagnetic energy needed to make an unforced particle relax to $1/e$ of any initial displacement from the center of the trap. The greater the optical power in the tweezers beam, the faster a trapped particle relaxes to the potential minimum.

For the set of measurements in which the power was varied, we first get $b = 59.48 \pm 0.27 \mu\text{J}$ from the best fit to the slope of $\omega_0 \times \tan(\phi_2/2)$ versus P . For the set of measurements in which the frequency was varied, we get $\tau = 1.290 \pm 0.003$ ms from the best fit to the slope of $\cot(\phi_2/2)$ versus ω_0 (see inset in Fig. 2), and using $P = 46$ mW we have $b = 59.73 \pm 0.15 \mu\text{J}$.¹³ For this set of measurements the trap constant is $\kappa = 1.38 \times 10^{-5} \pm 3.2 \times 10^{-8}$ N/m, where we used $\gamma = 1.79 \times 10^{-8}$ kg/s from the known viscosity and particle size. The main graph in Fig. 2 shows ϕ_2 versus $\omega_0\tau$ for both data sets for which we used $59.73 \mu\text{J}$ for the value of b . Also plotted is the theoretical line $\cot(\phi_2/2)$. One of the advantages of our technique is that it allows us to optimize the sensitivity of the measurement by varying P , ω_0 , or both, enabling us to make measurements over a large range of medium viscosities without changing the apparatus while keeping the SNR high, as can be seen from Eq. (5) below.

The results show that Eq. (4) holds and reaffirms the proportionality assumption between κ and laser power P . We also see that the parameter b is the same for both sets of measurements, which shows it is independent of both ω_0 and P as can be seen from Eq. (5) below. Changes in the value of b thus represent real changes in the medium viscosity and can be used to monitor biological, physical, or chemical processes.

To deduce the absolute viscosity of the fluid we need to measure the trap stiffness independently. This could be done either by another method, such as the escape force method,¹⁴ or by use of a standard medium for calibration. In many cases, only relative viscosities need to be determined, for example, in a cell-sorting application in which we are interested in the cell producing the highest viscosity in a given population. In cases in which an absolute measure-

ment is required, we can calibrate the system using materials of known viscosity, such as water or glycerol. Calibration against standards is preferred over *ab initio* calculations because we do not need to take into account the physical parameters of the probe particle or the inaccuracies of the available theory regarding the trap stiffness κ . Once calibration is done, we need only one measurement of the phase ϕ_2 to determine the viscosity of a given medium. If 3-D measurements are needed in an inhomogeneous medium, then calibration of the trap stiffness needs to account for the variation in depth inside the medium (see Section 6). We note that for accurate mapping of the viscosity, it is important that the variation in refractive index be small, such that the trap stiffness does not vary appreciably. If this is not the case, then the measurement is complicated by the inability of our method to decouple the change in index from the change in viscosity.

5. Signal-to-Noise-Ratio

A full analysis of the SNR of our measurement technique is given in Appendix A. Here we present the main ideas and the basic result from that research, which we believe is pertinent to understanding the advantages of the technique. The approach in the calculation is to look at the equation of motion of the particle and to include the Brownian motion as the main source of noise in the measurement under the assumption that the detector is not limited by the light intensity. The thermal excitation adds a randomly fluctuating component to the position of the particle. Since we are dealing with a linear system, the solution for the relative position u is a superposition of the purely sinusoidal function with low-pass filtered noise (the Lorentzian spectrum). A quadratic approximation to the confocal point-spread function (PSF) is used to relate the particle's displacement to the signal voltage. Since the detection is nonlinear in relative displacement u , we find a modulation of the thermal noise at frequency ω_0 by a signal-noise cross term that is the main source of noise at the narrow measurement band ($2\Delta\omega$) centered at $2\omega_0$. These considerations allow us to obtain an analytical expression for the viscosity SNR defined as $\text{SNR}_\eta \equiv \eta/\Delta\eta$, where $\Delta\eta$ is the rms fluctuation of the viscosity η ,

$$\text{SNR}_\eta = \frac{(\omega_0\tau)^2}{(\omega_0\tau)^2 + 1} \frac{\alpha}{\left(\frac{k_B T}{\kappa}\right)^{1/2}} \left(\frac{1}{8\Delta\omega\tau}\right)^{1/2}. \quad (5)$$

We first note that the SNR is proportional to the ratio between the amplitude of the oscillation α and the rms thermal fluctuations $(k_B T/\kappa)^{1/2}$. We also note that for long time constants or high trap oscillation frequencies, the SNR approaches a constant value. We can rearrange Eq. (5) and write

$$\text{SNR}_\eta = \frac{\text{SNR}_\eta^\infty}{1 + (\omega_0\tau)^{-2}},$$

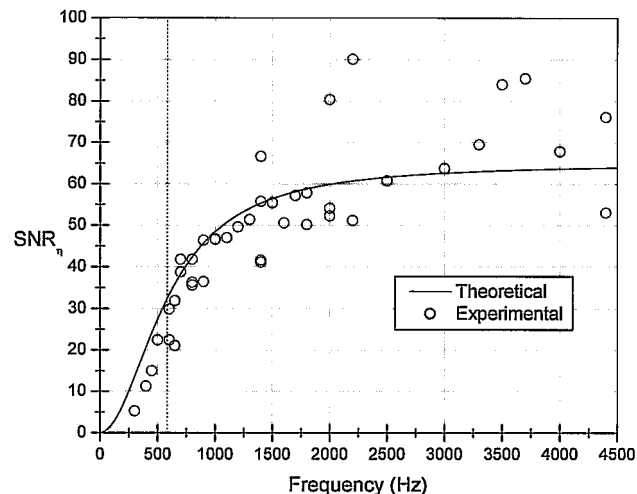


Fig. 3. SNR of the viscosity measurement for 0.9- μm -diameter silica microsphere in water with 18 mW of laser power at 815 nm and a constant NEBW of 2.6 Hz. The characteristic frequency $f_c = 585$ Hz is indicated by the dotted line. The solid curve is the theoretical curve (see text for details).

where

$$\text{SNR}_\eta^\infty = \frac{\sqrt{\frac{1}{2}} \kappa \alpha}{[2\gamma k_B T (2\Delta\omega)]^{1/2}} = \frac{F_{\text{spring}}^{\text{rms}}}{F_{\text{Langevin}}^{\text{rms}}}. \quad (6)$$

At high viscosities ($\omega_0\tau \gg 1$), for constant laser power, the sensitivity in the measurement of the viscosity saturates at a value (SNR_η^∞) that is given by the ratio of the rms spring force of the laser trap to the rms Langevin force in the bandwidth $2\Delta\omega$. In the other extreme in which $\omega_0\tau \ll 1$, the SNR increases like the square of the viscosity. We see that if we operate in the regime of high viscosity, we can reach high SNR where the only limiting factor is the amount of laser power that we have available (since κ is proportional to the laser power). However, if speed of measurement is of concern then, as shown in Eq. (5), we are also limited by the bandwidth of the LIA.

In a typical experiment the laser power at the sample plane is 18 mW at 815-nm wavelength. We use a 0.9- μm -diameter silica microsphere in water ($\eta = 1 \times 10^{-3}$ kg/m/s), an amplitude $\alpha = 100$ nm, $\kappa = 3.12 \times 10^{-5}$ N/m, and a bandwidth of 2.6 Hz, which is the noise-equivalent bandwidth (NEBW) of the LIA when it is set with a time constant of 30 ms and a filter slope of 24 dB/octave.¹⁵ Figure 3 shows the SNR measured under these conditions for a range of oscillation frequencies (the laser power and measurement bandwidth were kept constant). The time constant $\tau = 0.272 \pm 0.0014$ ms was found from a fit to Eq. (4). Values for the experimental SNR were calculated with $\text{SNR}_\eta = (\sin \phi_2)/\Delta\phi_2$ [derived by the definition of SNR_η and by Eq. (4)], in which we used the mean and standard deviation from 1024 samples of ϕ_2 (sampled at 64 Hz) for each data point.¹⁶ The theoretical SNR is also shown by the

solid curve, where we fitted Eq. (5) to the data with the free parameter $\text{SNR}_{\eta}^{\infty}$. The value of $\text{SNR}_{\eta}^{\infty}$ from the best fit to all the data points is 65, whereas the theoretical $\text{SNR}_{\eta}^{\infty}$ calculated with the parameters above is 46.5. The discrepancy might be accounted for by the uncertainty in the value for the oscillation amplitude a and variations in the laser output power.

The SNR sets a limit to the dynamic range of viscosities that can be accurately measured for a given optical power. We estimate the dynamic range using Eq. (5) to be of the order of 2 decades. For a fluid of viscosity 200 times that of water, the SNR drops to $\eta/\Delta\eta = 5$. This estimate assumes the following parameters: a 0.9- μm -diameter silica microsphere, an 800-nm trap wavelength, a $\kappa = 2 \times 10^{-5}$ N/m trap constant, an $f = 1100$ Hz tweezers oscillation frequency, a trap oscillation amplitude 0.14 μm , and a lock-in time constant 100 times the period of oscillation of the trap ($\Delta\omega = 5$ rad/s). Note that a larger dynamic range can be achieved by one's increasing the laser power or by one's reducing the detection bandwidth, but the latter comes at the expense of reduced speed. From Eq. (5) we see that by increasing the oscillation amplitude we can increase the SNR and as a result the dynamic range. Finally, we note that the SNR in the viscosity measurement is equivalent to the SNR in κ since

$$\text{SNR}_{\eta} = \frac{\eta}{\Delta\eta} = \frac{\gamma}{\Delta\gamma} = \frac{\kappa}{\Delta\kappa}.$$

If we know γ from *a priori* knowledge of particle radius and medium viscosity, then this equivalence of SNRs means that we can have a high-precision calibration of the transverse trap stiffness. For example, for an SNR of 65 in water, we get the value of κ with a precision of 1/65 or 1.5% by a single measurement of the second-harmonic phase, which takes about a second to complete.

6. Trap Stiffness

In confocal microscopy 3-D visualization is made possible by the depth discrimination property.^{7,17} This property allows us, in this setup, to drag the probe particle to deeper depths far from the cover glass and to obtain 3-D information of the viscosity distribution in a given medium. To do that, however, we need to first determine how the transverse trap stiffness (κ) varies along the axial (z) dimension. A complication that arises is the fact that objects moving close to a surface experience an increase in the drag due to the no-slip boundary condition. For a sphere moving in a viscous fluid near a surface, it was shown in Ref. 18 that the modification to the Stokes drag coefficient is given by a multiplicative factor involving the ratio of

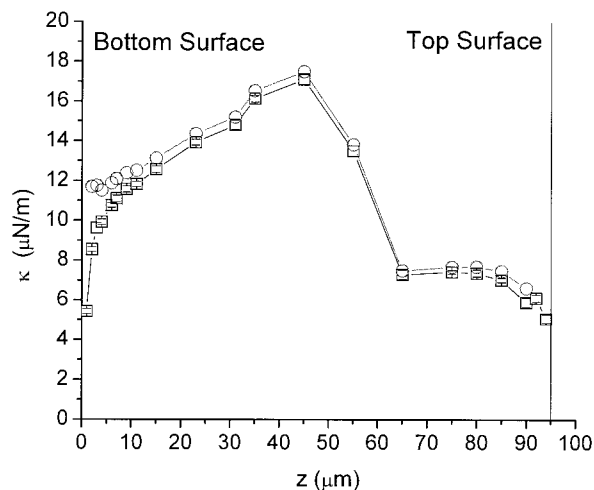


Fig. 4. Trap stiffness as a function of distance from the cover glass. κ is calculated by means of γ_{∞}/τ (□) and by means of $\gamma_{\infty}g(z)/\tau$ (○) with Brenner's formula for the correction near the two surfaces (see text). We obtain τ from measurements of the second-harmonic phase for the following conditions: 1.9- μm -diameter silica microsphere in water $\gamma_{\infty} = 6\pi\eta r = 1.79 \times 10^{-8}$ kg/s, constant laser power of 29 mW at the sample, 815-nm wavelength, constant frequency of oscillations of 500 Hz, objective lens 100 \times magnification, and 1.25 NA oil immersion. Solid lines are drawn to guide the eye. Each data point is the mean of 512 samples (sampled at 64 Hz where the time constant of the LIA was 300 ms and 0.26 Hz NEBW). Error bars obtained from the standard deviations.

the radius of the sphere (r) and its distance from the surface (z),

$$g(z) = \left[1 - \frac{9}{16} \left(\frac{r}{z} \right) + \frac{1}{8} \left(\frac{r}{z} \right)^3 - \frac{45}{256} \left(\frac{r}{z} \right)^4 - \frac{1}{16} \left(\frac{r}{z} \right)^5 \right]^{-1}. \quad (7)$$

Figure 4 shows results from a set of measurements of the second-harmonic phase taken at different distances (z) from the bottom cover glass. We increased z in steps by moving the objective lens assembly using a stepper motor actuator. We plot κ as a function of z by calculating γ_{∞}/τ , where $\gamma_{\infty} = 6\pi\eta r = 1.79 \times 10^{-8}$ kg/s is the value for the Stokes drag for 1.9- μm -diameter silica microsphere in water far from any surface. We also plot κ after correcting for the drag near the bottom (coverslip) and top (glass slide) surfaces by calculating $\gamma_{\infty}g(z)/\tau$. The correction factor is only important close to the surface, where the distance is of the order of the particle's radius.¹⁹ The figure reveals a complicated relation of the transverse trap stiffness dependency on z . We find that the trap stiffness initially increases approximately linearly with distance from the coverslip. It then falls sharply in the middle of the chamber and then stays relatively constant until another final decrease close to the top surface. The variation in trap stiffness, we believe, originates in the severe spherical aberrations that result from the use of an oil-

immersion objective lens. When the focus is immediately below the coverslip, there are minimal aberrations, but as the focus is moved further deep into the water, the ray paths do not converge since off-axis rays experience more refraction at the coverslip–medium interface.⁸ This results primarily in a decrease in axial trap efficiency, which moves the equilibrium position of the particle in the z direction further down the beam. This decrease, in turn, results in a change in transverse trapping since the particle experiences a different lateral gradient in the new z position.^{20,21} The interpretation of the trap stiffness measurements is not straightforward and is sometimes even counterintuitive.⁴ We find it rather surprising that the observed transverse trap stiffness actually increases with depth. This result suggests that as we increase z , the particle experiences a sharper gradient in intensity in the lateral (x – y) plane. Whatever the reason for this dependency, it is clear that it must be considered when the method is applied to measure viscosity in an inhomogeneous medium at different depths.

7. Discussion

A. Comparison with Other Methods

To the best of our knowledge, there has been no previous study of optical tweezers as a confocal probe to monitor the position of a particle relative to the center of an oscillating trap or the associated use of second-harmonic phase detection to obtain τ . Visscher and Brakenhoff²² combined optical tweezers with a confocal microscope but not in the same way and not for the same purpose. In that arrangement there were two separate paths for confocal imaging and laser trapping with two different objective lenses from opposite sides of the sample. Their device attempted to use the laser to keep an object trapped and to manipulate it while at same time supplying confocal scanning imaging of the field of view to a CCD camera. A special trap objective lens was constructed to allow the 3-D manipulation of the object by moving the effective lens inside the objective lens itself. Their device does not make use of confocal detection to measure the displacement of the particle from the trap center. The confocal part is used strictly for 3-D sectioning, and there is no attempt to measure τ .

There are numerous reviews in the literature of photonic force calibration techniques.^{4,14,23} Florin *et al.*²³ divide these methods into two main categories: one, calibration against known forces (such as Stokes friction and gravity) and two, analysis of thermal fluctuations. We can look at another subdivision for methods that require a well-calibrated position sensor of the trapped particle and methods that instead measure temporal changes in the signal and do not require an absolute distance measurement. Visscher *et al.*¹⁴ describe and compare the following methods: escape force, drag force, step response, power spectrum, and equipartition. With the exception of the last, all methods essentially measure τ . The

trap stiffness is derived from knowledge of γ ($\kappa = \gamma/\tau$), and one obtains force measurements by assuming a Hookian spring force for the trap and using a position sensitive detector. For accurate force measurements, both the trap stiffness and the position signal need to be well calibrated. For position detection most methods use a quadrant (or split) photodiode placed in an image plane. In one example, Florin *et al.*²³ use such detection to measure the position and use Boltzmann statistics to analyze the thermal noise and obtain the shape of the potential well of the trap. They deduce κ from the best fit to harmonic potential.

To make a fair comparison requires accounting for the purposes of each technique so that its advantages and disadvantages can be evaluated. Although our method could be used to calibrate the trap stiffness, it was developed specifically to be fast and robust for scanning the laser beam (as in confocal microscopy) and not for absolute position detection with the nanometer resolution, needed, for example, for picotensiometry.

Advantages of our technique stem from the following:

- The simplicity of the optical setup—its automatic alignment property and the solutions it provides for laser beam manipulation.
- The active use of photonic force to move the particle at high frequencies (kilohertz range) by the AOD.
- The highly sensitive detection of the particle's displacement from the trap center.
- The scanning capability and the large photon fluence at the detector, all resulting from the confocal geometry.
- The use of a digital LIA to accurately measure the second-harmonic phase with a narrow noise bandwidth, yielding a high SNR while maintaining a short data-acquisition time.
- The fact that, unlike the techniques of power spectrum and Boltzmann statistics, there is no need to fit the data in our measurement. This factor allows for a real-time measurement without complicated analysis.

Methods belonging to the category of thermal fluctuations, use the wide Brownian spectrum of the trapped particle to deduce the stiffness κ from the Lorentzian spectrum corner frequency f_c . The random fluctuations in the position of the particle are monitored typically by a position-sensitive quadrant photodiode arrangement.^{14,24,25} These methods could be used to measure microscopic viscosity in a similar way to that of our device. However, they are not suitable for fast scanning for two main reasons. First, they are not suited for beam scanning since as the trapping beam moves, the image of the particle moves off the center of the split photodiode. Therefore, they can scan the sample only using motors or piezoelements on the microscope stage, which are much slower than moving the laser itself. Secondly,

these methods are not fast owing to the long integration period inherent in a wideband spectral measurement. In most methods employing the position-sensitive detector, the trapped particle acts like a microlens that collimates the light. Different size particles have different effects on the light path, and as a result, realigning and recalibrating the position sensor is needed every time a new type of particle is trapped.

In our opinion the use of an active periodic forcing, rather than the use of the Brownian spectrum, is more adaptive to environmental constraints; large variations in the medium viscosity can be handled by the ability to change the trap stiffness or oscillation frequency. Our method does not rely on thermal excitations to supply the forcing; it shifts the measurement away from the thermal Lorentzian noise and the low-frequency mechanical noise spectra to a much higher frequency of our choice. For example, without special isolation from mechanical noise and sound, vibrations from environmental disturbances would be picked up by the system and would appear in the power spectra as peaks at the harmonic frequencies.

The technique described by Valentine *et al.*²⁶ is the one that is most similar to ours. They also use an active force rather than a thermal noise and measure the response of a particle to periodic forcing by optical tweezers employing lock-in detection. The main difference between their device and ours is the use of a split photodiode and not confocal detection for the particle's position. In addition, it is slower, as can be seen by considering the SNR.

Using similar considerations to the ones leading to Eq. (5), we calculated the SNR for the case of Valentine's device (see Appendix A) where we define $\omega_c = 1/\tau$:

$$\text{SNR}_{\eta}^{\text{Valentine}} = \frac{\omega_0 \omega_c}{\omega_0^2 + \omega_c^2} \frac{\alpha}{\left(\frac{k_B T}{\kappa}\right)^{1/2}} \left(\frac{\omega_c}{8\Delta\omega}\right)^{1/2}. \quad (8)$$

The ratio between the SNRs of the two methods is simply $\omega_0\tau$.

$$\frac{\text{SNR}_{\eta}^{\text{Confocal}}}{\text{SNR}_{\eta}^{\text{Valentine}}} = \omega_0\tau. \quad (9)$$

The advantage of applying high-oscillation frequency to the trap is the ability to make a quick measurement while integrating over many periods. This ability leads to the possibility of fast scanning viscosity microscopy.³ The shorter the integration time, the larger the measurement bandwidth. If we adjust the measurement bandwidth ($\Delta\omega$) to be proportional to the tweezers oscillation frequency (ω_0), the SNR is maximized when $\omega_0\tau = \sqrt{3}$ for the confocal case and when $\omega_0\tau = \sqrt{1/3}$ for Valentine's method.

In Fig. 5 we compare the signal-to-noise behavior of Valentine's device to ours by plotting the SNRs as a function of frequency using Eqs. (5) and (8). Notice that at low frequencies, Valentine's method is supe-

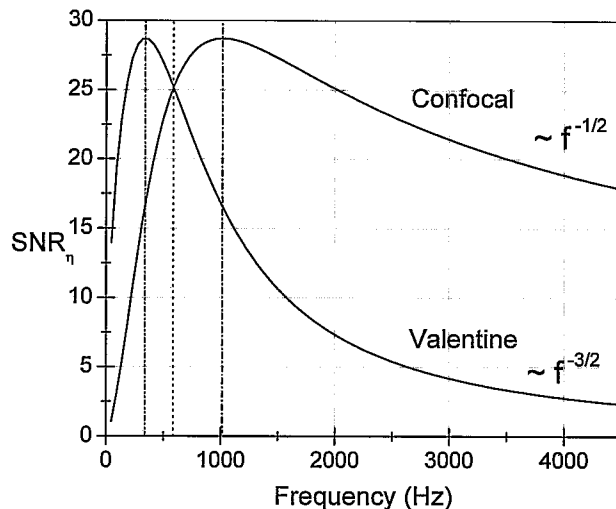


Fig. 5. Comparison of the theoretical SNR of the viscosity measurement for the confocal detection (our device) and for the split-photodiode position detection (Valentine's device). The measurement bandwidth was taken to be proportional to the oscillation frequency. The SNR of the two methods are equal at the characteristic frequency, which was taken to be $f_c = 585$ Hz (as used in Section 5). The confocal SNR peaks at $\sqrt{3}f_c = 1013$ Hz, whereas Valentine's SNR peaks at $1/\sqrt{3}f_c = 338$ Hz. The three frequencies are marked with dotted lines. From left to right these are the frequency of peak SNR for Valentine's device, the frequency where the SNR of Valentine's device is equivalent to ours, and the frequency of peak SNR for our device.

rior to ours, since the split photodiode ac signal is large when the bead can follow the trap, but the confocal ac signal is small since the particle stays close to the center of the trap. But at high frequencies, required for high data-acquisition rates, the confocal detection SNR significantly exceeds that of the split photodiode method. The SNR decreases as $\omega_0^{-1/2}$ in the confocal case but as $\omega_0^{-3/2}$ in the split photodiode case.

Florin *et al.*²⁷ combine optical tweezers and a two-photon fluorescence microscope to measure surface topography and stiffness. While they do not actively move the particle, they detect its position in a way similar to a confocal microscope. Their method eliminates the need for the pinhole, but it is limited by the need for an ultrafast laser.

Meller *et al.*²⁸ proposed the approach of localized dynamic light scattering (LDLS) on a particle trapped by optical tweezers. They compute the temporal autocorrelation function (ACF) of the scattered intensity and relate it to the particle position correlation function to obtain τ . In comparison with the other methods discussed, their method does not use a position sensor, but it requires careful alignment of the probe fiber and isolation from low-frequency noise that otherwise decreases the SNR. In addition, it requires a long integration time for the statistics to be reliable (a few minutes as compared with less than a second for our method³). There are, however, advantages in getting the position ACF, which can reveal the existence of more than one relaxation time,

since it probes a very wide spectral range (microseconds to seconds). In the case of complex fluids, the information in the ACF can be used to obtain the viscoelastic and shear modulus.²⁹

B. Possible Extensions of the Technique

In complex fluids such as gels or entangled polymer matrices, the viscoelastic properties are a function of frequency. Our method could be modified to include measurements of the frequency dependence of the viscosity, but this would detract from its speed. For complex fluids, the ACF does supply the relevant information. We can, however, apply the approach of LDLS to our device in a mode that uses the trap in a stationary position with no external forcing. The backscattered light signal is fed to an autocorrelator rather than the LIA. Compared with the optical fiber detection used by Meller *et al.*,²⁸ this arrangement is simpler, more robust, and provides a strong signal by the use of our confocal detection. The price for simplicity in optical design and implementation is the complexity of the data interpretation as noted by Kaplan *et al.*²⁹ In traditional dynamic light scattering we collect light at a particular wave vector and from a volume containing, in general, many particles or molecules that are free to move in and out of this volume.³⁰ By contrast, we have a single particle trapped in the tweezers, and the signal is made up of mixing of all wave vectors collected by the objective lens' high numerical aperture. Another complication in the data interpretation arises when we consider the 3-D nature of the fluctuations and the asymmetry in the axial versus lateral trapping. These factors lead to different relaxation times for lateral and axial motions, which are reflected in the shape of the ACF.

To simplify the interpretation of the ACF, we propose to view the fluctuations in the detected intensity as a random sampling by a point particle of the PSF of the confocal microscope. This is the same approach that was used in the derivation of the SNR, which seems to agree quite well with experiment. Thus the ACF of the confocal signal can be interpreted to first-order approximation as the ACF of the square of the displacement of a point particle from the geometric focal point. In many cases only the mean square fluctuations are important, so the fact that the confocal signal is insensitive to direction is unimportant, and we obtain all the relevant information.

As an example for the use of this detection model to obtain the ACF, we can look at the simple case of a particle in a stationary trap undergoing Brownian motion in a Newtonian fluid. If u is the displacement from the trap center, the fluctuations in position for a stationary trap result from the thermal noise. In this case $u(t) = N(t)$, where $N(t)$ is assumed to be wide-sense stationary (WSS) Gaussian

noise with a Lorentzian power spectral density and an exponentially decaying ACF,

$$R_N(t) = \overline{N(t) N(0)} = \frac{k_B T}{\kappa} \exp(-\omega_c |t|),$$

$$\text{where } \omega_c = 1/\tau \quad (10)$$

with a variance that is equal to the mean-square position fluctuations

$$\overline{N^2(t)} = R_N(0) = k_B T/\kappa.$$

Given these assumptions it can be shown that the ACF for the confocal signal from a Brownian particle in a stationary trap in a purely viscous medium is (see Appendix A)

$$R_{yy}(t) = \overline{y(t) y(0)} = \left(\frac{k_B T}{\kappa}\right)^2 \left(1 + 2 \exp\left(-2 \frac{|t|}{\tau}\right)\right), \quad (11)$$

where $y \equiv u^2$ is the time-varying confocal signal (for correlation functions, t denotes the delay time not actual time).

We believe that further research on the interpretation of the ACF from the confocal signal of trapped objects in different environments would make this mode of operation of the microscope very useful. This possibility could extend the capability of our device to microrheological measurements and to the study of the properties of complex fluids and systems such as Actin networks and entangled polymers.

Apart from rheological data, LDLS on trapped particles could open the door for a totally different type of experiment in which the trapped particle itself is the subject of interest. We can, for example, obtain information on the particle size from the ACF, or in the case of a live object, learn something about its state. For instance, it is quite easy to trap bacteria in the laser tweezers (near-infrared light is used to minimize photodamage). Since we expect the temporal statistics of the fluctuations in position of motile bacteria to be different from that of a nonmotile bacteria, we can use the ACF to differentiate between the two, and thus to distinguish between bacteria in different states, perhaps live or dead bacteria (although death in bacteria is not strictly defined by lack of motion). The reasoning is that for an inanimate object (such as a dead bacterium), trapped by the laser tweezers, the ACF should look like the Brownian particle's ACF, in which the hydrodynamic size is the important parameter determining the correlation time. However, for a motile bacterium in the trap, the temporal correlation in position would be affected by the additional independent motion, which is not purely random but is correlated for some short interval, and would therefore extend over longer delay times. The optical tweezers could be used to rapidly scan and interrogate different bacteria to determine which cells are alive or dead, or alternatively, we can apply different antibacterial substances to a single trapped bacte-

rium and monitor the ACF for changes, thereby testing the efficacy of the drugs.

Finally, we have recently shown³¹ that flow in the medium in the direction of oscillations, does not affect the second-harmonic phase but adds a fundamental frequency component, the magnitude of which is proportional to the flow velocity. The reason for this effect comes from the particle being pushed to one side by the drag force and the confocal detection being nonlinear. Thus, a measurement of the flow (in one dimension) as well as the viscosity of the medium can be done simultaneously.

Similarly, it can be shown that a constant force on the particle in the direction of the oscillation can be measured by use of the magnitude of the fundamental component. This fact could prove useful, for example, for measurements of the flexibility of single molecules, where the particle is pulled on one side by the force of the tweezers and on the other side by the tension force from the molecule being stretched.

8. Conclusion

We have presented a method to measure relative viscosity of a fluid on a microscopic scale. The combination of periodic forcing of trapped particles at high frequencies with confocal detection leads to a high SNR measurement, which facilitates fast scanning in three dimensions. Since the measurement is based on time and not distance, it requires no position calibration and is simpler to implement with the use of a phase-sensitive digital LIA.

We have developed a model to relate this phase lag to the medium viscosity and trap stiffness and demonstrated experimentally that the linear model holds by measuring the dependence of the second-harmonic phase angle on the frequency of oscillations and laser power. The results show excellent agreement between the experiment and the theoretical prediction.

A comparison to existing methods shows that our optical setup and detection technique allow fast data-acquisition and scanning capabilities, which are usually lacking in other techniques. We believe that these qualities of our device could make it a potentially important complementary imaging tool in such biological and medical applications that demand precision and high spatial and temporal resolution of viscosity distributions.

Appendix A

1. Relative Position-Sensing Signal-to-Noise Ratio—Confocal Detection

To calculate the SNR in the viscosity measurement, we include the Brownian motion since this is the main source of noise; the detector is not limited by the light intensity. The fluctuations in the signal can be traced back to the fluctuations in the position of the particle that gives rise to intensity fluctuations of the scattered light. The intensity fluctuations depend on the position fluctuations through the PSF of the optical system, the Gaussian beam profile, and the particle form and size.

In general, one needs to calculate a convolution integral of the PSF with the field amplitude at the plane of the particle and to take into account the wave vector dependency and the particle's curvature. For the sake of simplicity, supposing the bead stays close to the center of the trap, we can approximate the confocal signal as quadratic in the displacement u of the bead from the center of the trap.

$$I(t) \propto 1 - \alpha u^2(t), \quad (\text{A1})$$

where α is an expansion coefficient.

Our approach is to calculate the PSD of $y(t) = u^2(t)$ and to identify in it the contributions to the signal and the noise in our experiment. We start with Eq. (2), including the Langevin term $L(t)$,

$$\frac{du(t)}{dt} + \omega_c u(t) = \frac{L(t)}{\gamma} - a\omega_0 \cos \omega_0 t. \quad (\text{A2})$$

$L(t)$ is a random variable with the following properties³²:

1. It is a WSS process with zero mean $\overline{L(t)} = 0$ (where $\overline{[\cdot]}$ denotes ensemble average).
2. Its ACF is given by $R_{LL}(t') = \overline{L(t')L(0)} = q \delta(t')$, where $q \equiv 2\gamma k_B T$, k_B is Boltzmann's constant, and T is absolute temperature.
3. It has a Gaussian probability density function (PDF) with the variance given by $\overline{L^2(t)} = q$.
4. It is WSS white noise with a constant PSD

$$S_L(\omega) = \overline{|\tilde{L}(\omega)|^2} = q.$$

In terms of $\omega_c = 1/\tau$ the solution of Eq. (A2) is

$$u(t) = -u_0 \sin(\omega_0 t + \phi_1) + N(t), \quad (\text{A3})$$

where

$$u_0 = a\omega_0 / (\omega_c^2 + \omega_0^2)^{1/2}$$

$$\phi_1 = \cot^{-1}(\omega_0/\omega_c)$$

as in Eq. (3), where $N(t)$ represents the Brownian position fluctuations due to the stochastic forcing. It corresponds to filtered noise that is no longer white after passing through the low-pass filter formed by the restoring force of the trap. Like the input noise, it is a WSS Gaussian process with zero mean, but a PSD of a Lorentzian form,

$$S_N(\omega) = \overline{|\tilde{N}(\omega)|^2} = \frac{q}{\gamma^2(\omega^2 + \omega_c^2)} = \frac{2k_B T}{\gamma(\omega^2 + \omega_c^2)}$$

$$= \left(\frac{k_B T}{\kappa} \right) \frac{2\omega_c}{\omega^2 + \omega_c^2}, \quad (\text{A4})$$

(where we used $\kappa = \gamma\omega_c$). It has an exponentially decaying ACF

$$R_N(t') = \overline{N(t')N(0)} = \frac{k_B T}{\kappa} \exp(-\omega_c |t'|), \quad (\text{A5})$$

and a variance equal to the mean-square position fluctuations

$$\overline{N^2(t)} = R_N(0) = \frac{k_B T}{\kappa}.$$

The solution for the ac component of the confocal signal is

$$y(t) = u^2(t) = u_0^2 \sin^2(\omega_0 t + \phi_1) + N^2(t) - 2N(t) \times u_0 \sin(\omega_0 t + \phi_1). \quad (\text{A6})$$

The first term on the right-hand side of Eq. (A6) represents the signal in the detected intensity, and we denote it as y_S . We denote $y_{NN} \equiv N^2$ as the noise–noise term, and the last term y_{SN} as the signal–noise cross term. The Fourier transform of the signal is

$$\tilde{y}_S(\omega) = \frac{u_0^2}{4} [2\delta(\omega) + \delta(\omega - 2\omega_0)\exp j2\phi_1 + \delta(\omega + 2\omega_0)\exp -j2\phi_1]. \quad (\text{A7})$$

The PSD of the y_{NN} derived from standard theory³² is

$$S_{NN}(\omega) = \overline{|\tilde{y}_{NN}(\omega)|^2} = \left(\frac{k_B T}{\kappa}\right)^2 \left(\delta(\omega) + \frac{8\omega_c}{\omega^2 + (2\omega_c)^2}\right), \quad (\text{A8})$$

and its ACF R_{NN} is

$$R_{NN}(t') = \overline{y_N(t') y_N(0)} = \left(\frac{k_B T}{\kappa}\right)^2 [1 + 2 \exp(-2\omega_c|t'|)]. \quad (\text{A9})$$

The cross term $y_{SN} = 2N(t) u_0 \sin(\omega_0 t + \phi_1)$ can be treated as a modulation of the noise fluctuations by a sinusoid of frequency ω_0 , which results in a shift of the Lorentzian spectrum to that frequency.³³ Using Eq. (A4) results in the PSD of y_{SN} being

$$S_{SN}(\omega) = u_0^2 \overline{|\tilde{N}(\omega - \omega_0)|^2} = u_0^2 \left(\frac{k_B T}{\kappa}\right)^2 \frac{2\omega_c}{(\omega - \omega_0)^2 + \omega_c^2} \quad (\text{A10})$$

plus a similar expression for negative frequencies.

The amount of power in a small bandwidth $2\Delta\omega$ around the second harmonic $2\omega_0$ in signal, noise–noise, and signal–noise cross terms are respectively,

$$SP_{2\omega_0} = \frac{u_0^4}{8} = \frac{(a\omega_0)^4}{8(\omega_0^2 + \omega_c^2)^2}, \quad (\text{A11})$$

$$NP_{2\omega_0} = 4 \left(\frac{k_B T}{\kappa}\right)^2 \frac{\omega_c \Delta\omega}{\omega_0^2 + \omega_c^2}, \quad (\text{A12})$$

$$SNP_{2\omega_0} = \left(\frac{k_B T}{\kappa}\right)^2 \frac{4a^2 \omega_c \omega_0^2 \Delta\omega}{(\omega_0^2 + \omega_c^2)^2}. \quad (\text{A13})$$

The SNR in the magnitude of the component detected at $2\omega_0$ is given by

$$\text{SNR}_y = \left(\frac{SP_{2\omega_0}}{NP_{2\omega_0} + SNP_{2\omega_0}}\right)^{1/2}. \quad (\text{A14})$$

For all practical cases, $SNP_{2\omega_0}$ is much greater than $NP_{2\omega_0}$ (except for very small ω_0). The ratio of the square of the amplitude of the oscillation (a^2) to the mean-square thermal fluctuations ($k_B T/\kappa$) is usually of the order 100. Therefore, the pure noise term NP can be neglected in the SNR calculation and we conclude that

$$\text{SNR}_y \approx \left(\frac{SP_{2\omega_0}}{SNP_{2\omega_0}}\right)^{1/2} = \frac{a}{\left(\frac{k_B T}{\kappa}\right)^{1/2}} \frac{\omega_0}{\omega_c} \left(\frac{\omega_c}{32\Delta\omega}\right)^{1/2}. \quad (\text{A15})$$

The last approximation not only simplifies the expression for the SNR but is important for another reason. Although thermal fluctuations occur randomly in all three dimensions, the scalar product in the last term of Eq. (A6) ensures that only those fluctuations that are aligned with the axis of the oscillations of the trap will contribute to the noise in the measurement. The other fluctuations contribute only to the uncorrelated noise–noise term that we have neglected. Thus, the random movement of the particle in the z direction (parallel to the optical axis) will not considerably contribute to the noise in the measurement when the particle is forced to oscillate in the transverse direction. The insensitivity to motion in the z direction is a consequence of the square law detection, which is a unique feature of the confocal (relative) position sensing and of the fact that lock-in detection allows the measurement to be centered at frequencies away from those of the nonmodulated noise spectrum.

Assuming that the in-phase and quadrature noise are of equal magnitude, the uncertainty in the measured phase angle $\Delta\phi_2$ can be approximated by $\Delta\phi_2 \approx \tan^{-1}(\Delta y_{2\omega_0}/y_{2\omega_0})$, where $y_{2\omega_0}$ is the average (in the rms sense) amplitude measured by the LIA at $2\omega_0$ and $\Delta y_{2\omega_0}$ is the rms error (standard deviation from the mean). For large SNR (which is the case in our technique) we can safely make the small-angle approximation [$\tan^{-1}(\theta) \approx \theta$] and obtain

$$\Delta\phi_2 \approx \frac{\Delta y_{2\omega_0}}{y_{2\omega_0}} = \frac{1}{\text{SNR}_y}, \quad (\text{A16})$$

where $\Delta\phi_2$ is in radians).

To find the SNR in the viscosity measurement, defined as $\text{SNR}_\eta \equiv \eta/\Delta\eta$, we recall that the drag coefficient γ is proportional to viscosity. From our model

we know that $\gamma = (\kappa/\omega_0)\cot(\phi_2/2)$ [see Eq. (4)] and that a straightforward calculation shows that

$$\begin{aligned} \text{SNR}_\eta &= \text{SNR}_\kappa = \text{SNR}_\gamma = \frac{\gamma}{\Delta\gamma} = \frac{\sin \phi_2}{\Delta\phi_2} \\ &= \frac{2\omega_0\omega_c}{\omega_0^2 + \omega_c^2} \frac{1}{\Delta\phi_2} = \frac{2\omega_0\omega_c}{\omega_0^2 + \omega_c^2} \text{SNR}_y, \end{aligned} \quad (\text{A17})$$

which gives us the final result

$$\begin{aligned} \text{SNR}_\eta &= \frac{\omega_0^2}{\omega_0^2 + \omega_c^2} \frac{a}{(k_B T/\kappa)^{1/2}} \left(\frac{\omega_c}{8\Delta\omega} \right)^{1/2} \\ &= \frac{\text{SNR}_\eta^\infty}{1 + (\omega_c/\omega_0)^2}, \end{aligned} \quad (\text{A18})$$

where SNR_η^∞ is the SNR at the infinite oscillation frequency.

2. Absolute Position Sensing Signal-to-Noise Ratio—Valentine’s Method

We now turn to the SNR analysis for the device of Valentine *et al.*,²⁶ which uses a similar technique to periodically force the bead and measure its response. In that device, the bead is imaged directly onto a split photodiode, and the differential signal is used as an indicator of the position. This is a common method to sense microprobes positions in many optical tweezers-based experiments.

The derivation of the SNR is very similar; the main difference is that there is no cross term and that the magnitude of the noise and the signal is not squared since this is a linear detection of the position. However, since their device detects the absolute position, the amplitude of the signal decreases with frequency.

The equation of motion under periodic forcing for the position of the particle (x) with respect to a stationary reference at the origin is

$$\frac{dx(t)}{dt} + \omega_c x(t) = \frac{L(t)}{\gamma} + a\omega_c \sin \omega_0 t, \quad (\text{A19})$$

whose solution is given by

$$x(t) = x_0 \sin(\omega_0 t + \theta_1) + N(t), \quad (\text{A20})$$

where

$$x_0 = \frac{a\omega_c}{(\omega_0^2 + \omega_c^2)^{1/2}} \quad (\text{A21})$$

and

$$\theta_1 = -\cot^{-1} \left(\frac{\omega_c}{\omega_0} \right). \quad (\text{A22})$$

The noise PSD $S_N(\omega)$ is as in Eq. (A4). The noise power in a small band $\Delta\omega$ around ω_0 is

$$NP_{\omega_0} = \left(\frac{k_B T}{\kappa} \right) \frac{4\omega_c \Delta\omega}{\omega_0^2 + \omega_c^2}. \quad (\text{A23})$$

The mean-square amplitude of the sinusoid gives the power in the signal

$$SP_{\omega_0}^V = \frac{x_0^2}{2} = \frac{\omega_c^2 a^2}{2(\omega_c^2 + \omega_0^2)}. \quad (\text{A24})$$

The SNR in the rms amplitude x_{ω_0} is

$$\text{SNR}_x^V = \left(\frac{SP_{\omega_0}^V}{NP_{\omega_0}} \right)^{1/2} = \frac{a}{\left(\frac{k_B T}{\kappa} \right)^{1/2}} \left(\frac{\omega_c}{8\Delta\omega} \right)^{1/2}, \quad (\text{A25})$$

and as in Eq. (A16) we use $\Delta\theta_1 \approx \Delta x_{\omega_0}/x_{\omega_0} = 1/\text{SNR}_x^V$ (where $\Delta\theta_1$ is in radians).

From Equation (A22) we see that $\gamma = -(\kappa/\omega_0)\tan(\theta_1)$, yielding,

$$\begin{aligned} \text{SNR}_\eta^{\text{Valentine}} &= \frac{\gamma}{\Delta\gamma} = \frac{\sin 2\theta_1}{2\Delta\theta_1} \\ &= \frac{\omega_0\omega_c}{\omega_0^2 + \omega_c^2} \frac{1}{\Delta\theta_1} = \frac{\omega_0\omega_c}{\omega_0^2 + \omega_c^2} \text{SNR}_x^V, \end{aligned} \quad (\text{A26})$$

which gives us the final result

$$\text{SNR}_\eta^{\text{Valentine}} = \frac{\omega_0\omega_c}{\omega_0^2 + \omega_c^2} \frac{a}{\left(\frac{k_B T}{\kappa} \right)^{1/2}} \left(\frac{\omega_c}{8\Delta\omega} \right)^{1/2}. \quad (\text{A27})$$

We thank Joseph Noonan for useful discussions on the SNR and Amit Meller for his useful comments on LDLS.

References and Notes

1. K. Francis and B. O. Palsson, “Effective intercellular communication distances are determined by relative time constants for cyto/chemokine secretion and diffusion,” *Proc. Natl. Acad. Sci. USA* **94**, 12258–12262 (1997).
2. F. Yoshida, K. Horiike, and H. ShiPing, “Time-dependent concentration profile of secreted molecules in the intercellular signaling,” *J. Phys. Soc. Jpn.* **69**, 3736–3743 (2000).
3. B. A. Nemet, Y. Shabtai, and M. Cronin-Golomb, “Imaging microscopic viscosity with confocal scanning optical tweezers,” *Opt. Lett.* **27**, 264–266 (2002).
4. K. Svoboda and S. M. Block, “Biological applications of optical forces,” *Annu. Rev. Biophys. Biomol. Struct.* **23**, 247–285 (1994).
5. Some axial offset is required since the particle is trapped slightly after the geometric focal point of the laser. In one realization of the optical design, the pinhole is replaced by a single-mode fiber, and the lens in front of it is replaced with a fiber collimator. Use of an optical fiber instead of a pinhole is sometimes more convenient since it allows us to switch from an avalanche photodiode, which gives an analog signal, to a photomultiplier tube with a built-in pulse discriminator, which gives the digital photon count signal needed for the autocorrelator board during DLS measurements. Thus the switching involves no realignment of the optics.
6. Instruments: AOD (Model AOM 1205C-2, Isomet Corporation, Springfield, Va.); objective lens (oil immersion 100×, 1.25 NA semiplan, Edmund Industrial Optics, Barrington, N.J.); digital LIA (Model SR850, Stanford Research Systems, Sunnyvale, Calif.); galvanometer SMs (Model Z1913), servo controller (Model DX2003), and control bus (Model DG1003) (GSI Lu-

- monics, Ottawa, Ontario); laser (cw Ti:Sapphire laser, Model 3900S, pumped by Argon Ion laser stabilite 2017, Spectra Physics, Mountain View, Calif.); APD (Model C5460-01, Hamamatsu, Bridgewater, N.J.); CCD camera (Model 4915-2000, COHU, Inc., San Diego, Calif.) frame grabber (Model DT3155, Data Translation, Inc., Marlboro, Mass.); microscope cover glass (No. 1 Fisherfinest, Fisher, Pittsburgh, Pa.); Microspheres—uniform silica microspheres (Bangs Laboratories, Inc., Fishers, Indiana); and dc motor actuator (Model 850, Newport, Inc., Irvine, Calif.).
7. J. B. Pawley, ed., *Handbook of Biological Confocal Microscopy* (Plenum, New York, 1995).
 8. C. J. R. Sheppard and D. M. Shotton, *Confocal Laser Scanning Microscopy* (Springer, New York, 1997).
 9. The back focal plane that is the desired plane is ~ 20 mm inside most objective lens packages (unless an infinity-corrected lens is used); therefore, a compromise must be made for steering without light loss and vignetting effects.
 10. Similar analysis can be applied to the axial direction if the beam is set to oscillate axially. Since the confocal detection is sensitive to displacements in z as well as in x and y , the axial trap stiffness can be determined.
 11. A. J. Levine and T. C. Lubensky, "One and two-particle micro-rheology," *Phys. Rev. Lett.* **85**, 1774–1777 (2000).
 12. M. Doi, *Introduction to Polymer Physics* (Oxford University Press, New York, 1996).
 13. Before any analysis, the phase data was corrected for the overall system time delay that exists regardless of the motion of the particle. By observing the signal from a static reflective edge, we found experimentally that the fundamental phase decreases linearly as we increase the frequency with a proportionality time constant of $4.017 \mu\text{s}$, which is the time delay of the system (the response of the AOD and the rest of the electronics). At low frequencies this proportionality time constant adds an unnoticeable phase delay, but as we go to high frequencies, this additional delay becomes large, and a systematic deviation from the theoretical line appears. The second-harmonic phase was corrected as follows $\phi_2^{\text{corr}} = \phi_2^{\text{meas}} + 2\omega_0(4.017 \times 10^{-6})$ where ϕ_2 is in radians. Also note that in the model we use a sin function as the reference, but the LIA measures the in-phase component as the cos function; we therefore add $\pi/2$ to the measured phase before we apply the analysis using our convention.
 14. K. Visscher, S. P. Gross, and S. M. Block, Construction of multiple-beam optical traps with nanometer-resolution position sensing. *IEEE J. Sel. Top. Quantum Electron.* **2**, 1066–1076 (1996).
 15. Both the time constant and the slope of the low-pass filter at the reference frequency determine the actual NEBW. A sharper slope results in a smaller NEBW, allowing faster measurement for a given LIA time constant.
 16. Sampling faster than 64 Hz is, of course, possible but under the conditions of the experiment would lead to underestimating the standard deviation since we would be sampling much faster than the response of the LIA, and the sampled points would not be reflecting the randomness of the noise. This underestimation, however, would not affect the result for the mean value.
 17. T. Wilson and C. Sheppard, *Theory and Practice of Scanning Optical Microscopy* (Academic, London, 1984).
 18. J. Happel and H. Brenner, *Low Reynolds Number Hydrodynamics with Special Applications to Particulate Media* (Prentice-Hall, Englewood Cliffs, N.J., 1965).
 19. In the graph of the corrected κ we decided to omit the end-points that, owing to the uncertainty in the exact z position ($\sim 1 \mu\text{m}$), give unreasonably large values close to the singularity at $z = 0$ (and at $z = 95$, the top surface).
 20. A. Ashkin, "Forces of a single-beam gradient trap on a dielectric sphere in the ray optics regime," *Biophys. J.* **61**, 569–582 (1992).
 21. W. H. Wright, G. J. Sonek, and M. W. Berns, "Parametric study of the forces on microspheres held by optical tweezers," *Appl. Opt.* **33**, 1735–1748 (1994).
 22. K. Visscher and G. J. Brakenhoff, "Single beam optical trapping integrated in a confocal microscope for biological applications," *Cytometry* **12**, 486–491 (1991).
 23. E. L. Florin, A. Pralle, E. H. K. Stelzer, and J. K. H. Horber, "Photonic force microscope calibration by thermal noise analysis," *Appl. Phys. A: Mater. Sci. Process.* **66**, S75–S78 (1998).
 24. A. Pralle, E. L. Florin, E. H. K. Stelzer, and J. K. H. Horber, "Local viscosity probed by photonic force microscopy," *Appl. Phys. A: Mater. Sci. Process.* **66**, S71–S73 (1998).
 25. G. V. Shivashankar, G. Stolovitzky, and A. Libchaber, "Back-scattering from tethered bead as a probe of DNA flexibility," *Appl. Phys. Lett.* **73**, 291–293 (1998).
 26. M. T. Valentine, L. E. Dewalt, and H. D. Ou Yang, "Forces on a colloidal particle in a polymer solution: a study using optical tweezers." *J. Phys. Condens. Matter* **8**, 9477–9482 (1996).
 27. E. L. Florin, J. K. H. Horber, and E. H. K. Stelzer, "High-resolution axial and lateral position sensing using two-photon excitation of fluorophores by a continuous-wave Nd alpha YAG laser," *Appl. Phys. Lett.* **69**, 446–448 (1996).
 28. A. Meller, R. Bar-Ziv, T. Tlusty, E. Moses, J. Stavans, and S. A. Safran, "Localized dynamic light scattering: a new approach to dynamic measurements in optical microscopy," *Biophys. J.* **74**, 1541–1548 (1998).
 29. P. D. Kaplan, V. Trappe, and D. A. Weitz, "Light-scattering microscope," *Appl. Opt.* **38**, 4151–4157 (1999).
 30. B. J. Berne and R. Pecora, *Dynamic Light Scattering with Applications to Chemistry, Biology, and Physics* (Dover, New York, 2000).
 31. B. A. Nemet and M. Cronin-Golomb, "Microscopic flow measurements with optically trapped microprobes," *Opt. Lett.* **27**, 1357–1359 (2002).
 32. A. Papoulis, *Probability, Random Variables, and Stochastic Processes*, 3rd ed. (McGraw-Hill, New York, 1991).
 33. S. Haykin, *Communication Systems*, 2nd ed. (Wiley, New York, 1983).